# Crystal Structures of Brain Group-VIII Phospholipase A2 in Nonaged Complexes with the Organophosphorus Nerve Agents Soman and Sarin[†,‡]

Todd M. Epstein,[§] Uttamkumar Samanta,[§] Stephen D. Kirby,[#,§] Douglas M. Cerasoli,[#] and Brian J. Bahnson*[,§]

*Department of Chemistry & Biochemistry, University of Delaware, Newark, Delaware 19716, and U.S. Army Medical Research Institute of Chemical Defense, Aberdeen Proving Ground, Maryland 21010*

*Received December 23, 2008; Revised Manuscript Received February 16, 2009*

ABSTRACT: Insecticide and nerve agent organophosphorus (OP) compounds are potent inhibitors of the serine hydrolase superfamily of enzymes. Nerve agents, such as sarin, soman, tabun, and VX exert their toxicity by inhibiting human acetycholinesterase at nerve synapses. Following the initial phosphonylation of the active site serine, the enzyme may reactivate spontaneously or through reaction with an appropriate nucleophilic oxime. Alternatively, the enzyme−nerve agent complex can undergo a secondary process, called "aging", which dealkylates the nerve agent adduct and results in a product that is highly resistant to reactivation by any known means. Here we report the structures of paraoxon, soman, and sarin complexes of group-VIII phospholipase A2 from bovine brain. In each case, the crystal structures indicate a nonaged adduct; a stereoselective preference for binding of the $P_SC_S$ isomer of soman and the $P_S$ isomer of sarin was also noted. The stability of the nonaged complexes was corroborated by trypsin digest and electrospray ionization mass spectrometry, which indicates nonaged complexes are formed with diisopropylfluorophosphate, soman, and sarin. The $P_S$ stereoselectivity for reaction with sarin was confirmed by reaction of racemic sarin, followed by gas chromatography/mass spectrometry using a chiral column to separate and quantitate each stereoisomer. The $P_S$ stereoisomers of soman and sarin are known to be the more toxic stereoisomers, as they react preferentially to inhibit human acetylcholinesterase. The results obtained for nonaged complexes of group-VIII phospholipase A2 are compared to those obtained for other serine hydrolases and discussed to partly explain determinants of OP aging. Furthermore, structural insights can now be exploited to engineer variant versions of this enzyme with enhanced nerve agent binding and hydrolysis functions.

Organophosphorus (OP) compounds such as nerve agents interfere with the catalytic activity of serine hydrolases by forming a covalent phosphorus conjugate. OP compounds are believed to exert toxicity primarily through the inhibition of acetylcholinesterase (AChE), which is responsible for degrading the neurotransmitter acetylcholine. A larger superfamily of serine hydrolases have been shown to be inactivated by OPs, with potential clinical consequences (*1*). In each of these active sites, the serine residue is postulated to react with OPs by a $S_N2$ mechanism with a trigonal bipyramidal transition state. Upon loss of the displaced leaving group, stereoinversion at the chiral phosphorus atom occurs (*2*). Depending on the enzyme, the initial covalent phosphonylated complex can often be reactivated with a strong nucleophile, such as an oxime. Recently, efforts have focused on engineering cholinesterase enzymes to hydrolyze pesticides and nerve agents, and therefore function as catalytic OP[1] bioscavengers (*3*).

When bound to AChE, OP compounds with a branched side-chain at the $C_\alpha$ adjacent to the phosphoester typically undergo a dealkylation process known as aging (*4, 5*). The consensus mechanism for aging is believed to go through a carbocation intermediate as shown in Figure 1, and is dependent on the presence of both a branched chain in the OP adduct and an appropriately positioned proton donor in the enzyme. Following aging, the covalently inhibited enzyme cannot typically be reactivated by nucleophiles to regenerate enzymatic activity. Consistent with predicted carbocation stability, the aging rate is fastest for branched groups with a tertiary $C_\alpha$ group. This property of branched OPs makes them particularly resistant to conventional therapeutic approaches to OP intoxication.

The crystal structure of AChE was previously solved in complex with the nerve agent VX in a nonaged form (*6*).

[†] This work was supported by NIH Grants 2P20RR015588 from the National Center for Research Resources and 1R01HL084366-A1 from the National Heart, Lung, and Blood Institute.

[‡] Protein Data Bank entry codes 3DT6, 3DT9, and 3DT8 are nonaged group-VIII phospholipase A2 complexes with paraoxon, soman, and sarin, respectively.

* To whom correspondence should be addressed: Telephone: (302) 831-0786. Fax: (302) 831-6335. E-mail: bahnson@Udel.edu.

[§] University of Delaware.

[#] U.S. Army Medical Research Institute of Chemical Defense.

[1] Abbreviations: AChE, acetylcholinesterase; AH, acetylhydrolase; BChE, butyrylcholinesterase; CE1, carboxylesterase 1; ESI, electrospray ionization; GC, gas chromatography; MS, mass spectrometry; OP, organophosphorus; PAF, activating factor; PNPA, *p*-nitrophenylacetate; sarin, methylethyl methylphosphonofluoridate; soman, *O*-pinacolyl methylphosphonofluoridate; tabun, ethyl *N,N*-diemthylphosphoramidocyanidate; TCEP, triscarboxyethylphosphine; VX, *O*-ethyl *S*-(2-diisopropylaminoethyl) methylphosphonothiolate; 2-PAM, pyridine-2-aldoxime methochloride.

10.1021/bi8023527 CCC: $40.75 
Published on Web 03/09/2009

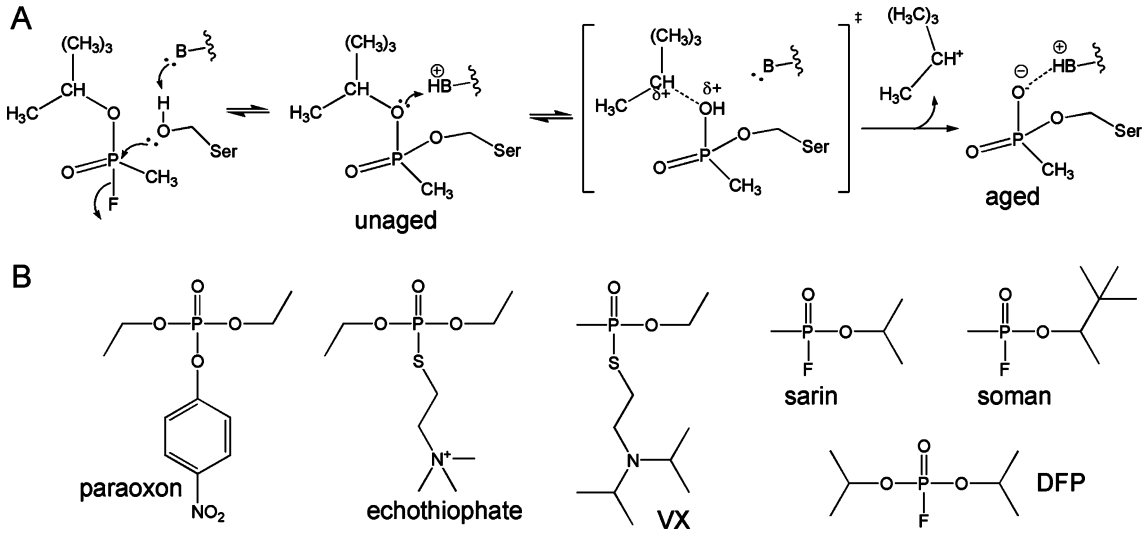


FIGURE 1: The reaction of a serine hydrolase with organophosphate compounds can stop at a nonaged complex or proceed to an "aged" complex through a carbocation mechanism. (A) The nucleophilic serine attacks the organophosphate compound first generating a stable tetrahedral serine-phosphoester "non-aged" intermediate. The "B" represents the active site His-Asp dyad. Protonation catalyzed by the enzyme promotes dealkylation through charge separation. Aging is promoted by a secondary or tertiary $C_\alpha$, which stabilizes the developing positive charge. In the AChE reaction, aging produces a negatively charged adduct that participates in a hydrogen bond with the active site histidine. The aged complex is resistant to reactivation by nucleophilic attack, while it is generally possible for the nonaged complex to be reactivated by outside nucleophiles, such as oximes. (B) The organophosphate compounds sarin, soman, and DFP have a branched alkyl side-chain at the $C_\alpha$ position that facilitates aging, whereas paraoxon, echothiophate, and VX do not, and are therefore more resistant to aging.

Additionally, Nachon et al. have reported the nonaged structure of human butyrylcholinesterase (BChE) with echothiophate, which was obtained by soaking ligand-free crystals with the OP inhibitor followed by immediate flash cooling of the crystal and X-ray diffraction data collection (*7*). Although VX and echothiophate have a propensity to age, the leaving group is unbranched at the $C_\alpha$ position, suggesting that this is a relatively slow reaction. There is a report of the serine protease factor D inhibited with diisopropylfluorophosphate (DFP) in a nonaged complex; however, factor D is an atypical serine protease where a conformational change is necessary to orient the active site histidine in a position to carryout activity (*8*). Recently, human carboxylesterase 1 (CE1) was reported to form nonaged complexes with the OPs soman and tabun, which are both branched at $C_\alpha$ (*9*).

Aging rates of OP compounds have been studied in a variety of systems: AChE (*10, 11*), BChE (*7, 10*−*12*), chymotrypsin (*13, 14*), subtilisin (*13*), and atropinesterase (*13*). Aging rates have a complex dependence on the specific enzyme−OP inhibitor system, pH, and temperature. Measured aging half-lives of enzyme−OP inhibitor complexes range from 10 days for the chymotrypsin−DFP complex (*13*) to 1 min for the AChE−soman complex (*11*). Typically, aging is a slow process that is enhanced in the case of the human AChE and BChE, which share 55% sequence identity. Hypotheses to explain this enhancement in aging rates include variation of the mobility of the active site histidine (*3*) and cation-$\pi$ interactions between the OP-adduct and aromatic residues in the choline binding pocket of the active site (*11*). Also E202 in human AChE is thought to play a role in "aging" in the cholinesterases (*15*).

The group-VIII phospholipase A2 (gVIII-PLA2) enzyme from bovine brain has been previously described as a 26 kDa intracellular catalytic domain that is also referred to as type-Ib platelet activating factor (PAF) acetylhydrolase (AH) (*16*). Although the structure of bovine gVIII-PLA2 has been reported (*17, 18*), there is no sequence homology to the other PAF-AH enzymes. Additionally, gVIII-PLA2 has been suggested to have a physiological function other than as a true PAF-AH enzyme (*19, 20*). In addition to developing gVIII-PLA2 as a potential OP bioscavenger, the present study provides mechanistic clues to specific enzyme−substrate contacts which can address whether gVIII-PLA2 is a PAF-AH or not. From previously reported work, the initially reported crystal structure contained an acetate ion from the crystallization buffer bound into a pocket formed by L48, T103, and L194. It was suggested that this bound acetate represents the mechanistically relevant position of substrate in the acetyl-binding pocket responsible for the enzyme's chain length specificity, which strongly prefers a short alkyl chain at this position (*17*). The structures of the gVIII-PLA2:OP complexes reported here yield additional information about the important interactions of active site residues. Crystal structures covalently inhibited by the OP compounds paraoxon, soman, and sarin were solved with diffraction data to a resolution of 2.1, 1.85, and 1.85 Å, respectively. Each structure reported provides convincing evidence of nonaged complexes, and in the case of soman and sarin a clear stereoselective preference of reaction. Results from mass spectrometry experiments corroborate the crystallographic results as they also indicate a stereoselective preference, and they showed no signs of an aged enzyme several days after inhibition with OP compounds.

## MATERIALS AND METHODS

*Expression and Purification of gVIII-PLA2.* Group-VIII-PLA2 was prepared as reported in detail previously (*20*). Briefly, cDNA for bovine gVIII-PLA2 was subcloned into the expression plasmid pGEX-4T1 (Amersham Biosciences) utilizing the *Eco*RI and *Sal*I restriction sites transformed into

DH5α cells. The GST-gVIII-PLA2 fusion protein was expressed in 2-L cultures grown at 37 °C until an optical density of 0.3−0.5 was reached at 600 nm, and protein expression was then induced by the addition of IPTG to a concentration of 0.5 mM. Cell lysate was cleared by centrifugation and the supernatant was loaded onto a 5 mL HiTrap Glutathione sepharose column (Amersham Biosciences). The column was equilibrated with 25 mL of 10 mM Tris, pH 8.0, 1 mM DTT and bound fusion protein was digested via on-column cleavage with the addition of 100 units of thrombin protease (Human Research Laboratories). Digestion was typically allowed to proceed overnight at room temperature. After digestion, cleaved gVIII-PLA2 was eluted with 10 mM Tris, pH 8.0, 1 mM DTT. The protein was then loaded onto a HiLoad 16/60 Superdex 75 (Amersham Biosciences) size exlusion column equilibrated with 20 mM Tris, pH 8.0, 1 mM DTT. Protein was concentrated to 5−6 mg/mL using an Ultra-10 ultrafiltration cell (Amicon) and buffer exchanged into 10 mM Tris, pH 8.0, 2 mM triscarboxyethylphosphine (TCEP) using an Econo-Pac 10 DG buffer exchange column (Biorad).

*Inhibition and Crystallization of gVIII-PLA2.* Inhibition with paraoxon was performed by adding 1 μL of a 100 mM paraoxon stock in ethanol to 40 μL of concentrated gVIII-PLA2. Inhibition was rapid, and was confirmed by checking activity with the substrate *p*-nitrophenylacetate (PNPA). Soman and sarin are highly controlled nerve agents and inhibition was performed at the U.S. Army Medical Research Institute of Chemical Defense located on the Aberdeen Proving Grounds in Aberdeen, Maryland. The procedures followed an approved safety protocol for moving material after the inhibition of gVIII-PLA2 was completed. A few microliters of dilute soman or sarin in saline solution was added to 40 μL of 5−6 mg/mL gVIII-PLA2 in 10 mM Tris, pH 7.4. The reaction was set up with a 2−4-fold molar excess of soman or sarin added for each inhibition experiment and a total amount of approximately 10 nmol of the inhibitor, well below amounts that are considered hazardous. The sarin inhibited gVIII-PLA2 rapidly while soman needed to be incubated on ice for approximately 3 h to achieve complete inhibition as measured by the loss of enzymatic activity using the substrate PNPA.

The inhibited enzyme solution was used directly for crystallization without any further processing. Crystallization conditions were the same as for the structure reported by Ho et al. (*17*). Protein crystallization hanging drops were made by addition of 2 μL of 5−6 mg/mL inhibited gVIII-PLA2 mixed with 2 μL of 16% saturated ammonium sulfate, 200 mM sodium acetate buffer, pH 6.5 and suspended over a reservoir solution of 500 μL of 16% saturated ammonium sulfate, 200 mM sodium acetate buffer, pH 6.5 at 25 °C. Crystals appeared after 2−3 days. Crystals were allowed to grow for two weeks at 25 °C before being equilibrated in cryo-protectant solution made up of the crystallization reservoir solution with xylitol. Crystals were prepared for data collection by first adding approximately 20 μL of the reservoir solution to the drop containing the crystals. Then 5 μL of solution was removed from the drop and replaced with 5 μL of reservoir solution supplemented with 40% saturating xylitol. This iterative process brought the crystals stepwise into a cryo-protected solution. Crystals were allowed to equilibrate for several minutes between each cryo solution exchange step. After six exchanges, the crystals were flash-frozen in liquid nitrogen and a −180 °C nitrogen cryostream was used during data collection.

*X-ray Data Collection and Crystal Structure Solution.* X-ray diffraction data was collected from a single crystal for each complex on a Rigaku RU-H3R rotating anode generator and a RAXIS IV image plate area detector. Data was processed in the space group $P3_121$ for all complexes using the program HKL2000 (*21*). The structure of group-VIII PLA2 (PDB entry 1WAB, gi: 27807201 (*17*)) was used as a starting model for the structure solutions, and refinement was accomplished using the programs CNS (*22*) and REFMAC5 (*23*). Model building and modifications have been carried out by using the graphics programs O (*24*) and coot (*25*). The final crystal structure solution consisted of one enzyme subunit in the asymmetric unit with the 2-fold symmetry axis of the dimer coinciding with the crystallographic 2-fold axis of space group $P3_121$. Unassigned difference electron density contiguous with active site S47 was identified in $3F_o - 2F_c$ difference electron density maps in all three complexes and determined to be the covalently attached OP inhibitor. In all structures, difference electron density allowed the unambiguous modeling of the OP adducts in a nonaged form. In each structure, occupancy refinement suggested 100% occupancy of the nonaged inhibitor. Models were initially refined with the program CNS (*22*), and then refined with the program REFMAC5 (*23*). A CIF parameter file for the nonaged complexes formed after reaction with paraoxon, soman and sarin was prepared using the monomer library sketcher module of the program CCP4 (*26*).

*Mass Spectrometry of Trypsin Digests.* Although the crystallographic data gave convincing evidence for the presence of nonaged complexes with soman and sarin, it was decided to investigate the presence of a nonaged complex via mass spectrometry analysis of tryptic peptides to detect the modification of S47. Electrospray ionization mass spectrometry analysis was done on complexes of gVIII-PLA2 with soman, sarin, and DFP. DFP was included as a positive control for the mass spectrometry investigation since it is a commercially available branched OP that is known to age at a fast rate in complexes with AChE and BChE (*27*).

Inhibition of gVIII-PLA2 with soman and sarin was performed at the U.S. Army Medical Research Institute of Chemical Defense as described above for the inhibition of protein crystals. The inhibition of gVIII-PLA2 was accomplished by adding 2−4 μL of 10 mM DFP stock in anhydrous isopropanol to 40 μL aliquots of gVIII-PLA2 in 10 mM Tris, pH 8. Inhibition with DFP was rapid, and was confirmed via inhibition of activity using the substrate PNPA. Inhibited gVIII-PLA2 was incubated at 4 °C for at least 48 h before proceeding to trypsin digestion for mass spectrometry analysis.

All samples, including a control sample, which was not inhibited, were buffer exchanged into 50 mM ammonium bicarbonate using Bio-Gel *P*4 micro spin buffer exchange columns (BioRad) in order to remove any residual OP compound that could interfere with trypsin digestion. Five microliter aliquots of buffer exchanged, inhibited gVIII-PLA2 were removed for trypsin digestion (approximately 25 μg of gVIII-PLA2). Samples were heated at 80 °C for 2 min followed by evaporation to dryness with a Savant Speed

Vac. Samples were reconstituted by adding 20 μL of 8 M urea, 0.4 M ammonium bicarbonate. Cysteine residues were reduced with the addition of 5 μL of 10 mM DTT. After incubation with DTT for 15 min, cysteines were blocked with the addition of 5 μL of 100 mM iodoacetamide followed by 15 min of incubation. Fifty μL of distilled and deionized $H_20$ was added to dilute the buffer composition to 2 M urea, 0.1 M ammonium bicarbonate, 0.625 mM DTT, and 6.25 mM iodoacetamide. Sequencing grade trypsin (Sigma) was reconstituted with 50 mM ammonium bicarbonate to a concentration of 1 mg/mL; trypsin was stored frozen at −20 °C and used within one week. Approximately 10% trypsin by weight (2 μg of trypsin) was added to each sample and incubated overnight at 37 °C. The pH was adjusted to 8.5 using 1 M ammonium bicarbonate before incubation.

After digestion, tryptic peptides were buffer exchanged and concentrated using ZipTip $C_{18}$ reverse phase pipet tips (Millipore). Ten microliters of each 80 μL digestion was taken for ZipTip cleanup. Samples were acidified with the addition of 1−2 μL of 10% trichloroacetic acid (TCA). The samples were then bound by repeat aspiration onto the ZipTips and washed according to the manufacturer's protocol. Samples were eluted in 4 μL of 40% methanol, 0.1% TCA. Samples were analyzed via direct injection into an electrospray ionization (ESI) mass spectrometer without prior chromatography separation. Interpretable mass spectra with high sequence coverage and a peptide containing S47 were obtained for all OP-inhibited complexes.

*Analysis of Stereoselectivity by Reaction with Racemic Sarin.* We have studied the stereoselectivity of sarin binding to gVIII-PLA2 by gas chromatography/mass spectrometry (GC/MS) methods modified from Yeung et al. (*28*). Assays were performed at the U.S. Army Medical Research Institute of Chemical Defense, Aberdeen Proving Grounds under controlled conditions. A 50 μL sample of purified gVIII-PLA2 (∼385 μM) or buffer (10 mM potassium phosphate, pH 7.4) were incubated for 30 min at room temperature with ∼600 nM racemic sarin (diluted from a 13.6 mM stock solution). After incubation, the samples were extracted with an equal volume of dry ethyl acetate supplemented with 50 μM DFP as an internal standard (not shown). The majority of the organic layer containing the unbound sarin was removed and passed over type 4A (grade 514) aluminasilicate molecular sieve to remove excess water. Samples were transferred to 11 mm crimp top vials for GC/MS analysis. One μL samples were passed through an Agilent 6890 gas chromatograph fitted with a 20 m × 0.25 mm inside diameter Chiraldex gamma-cyclodextrin trifluoroacetyl column with 0.125 μm film thickness (Advanced Separation Technologies, Inc.). The GC was interfaced to an Agilent 5973 mass spectrometer with an electronic impact ion source under selected ion monitoring mode. Two ions (*m*/*z* 99 and 125) were monitored for sarin quantitation and two additional ions (*m*/*z* 101 and 127) were monitored for DFP quantitation. The total area (data not shown) under the curves shown in Figure 5 was used to develop ratios of each isomer between samples.

*Reactivation Attempts with Oxime.* Group VIII-PLA2, which had been inhibited with DFP, was incubated with pyridine-2-aldoxime methochloride (2-PAM) in an attempt to reactivate the covalently inhibited enzyme. Inhibited gVIII-PLA2 was prepared, as described above. Twenty microliters of 5.6 mg/mL gVIII-PLA2 in 10 mM Tris, pH 7.4, 1 mM TCEP was inhibited by the addition of 0.5 μL of 20 mM DFP in isopropanol, and buffer exchanged into 10 mM Tris, pH 8.0 using Bio-Gel *P*4 micro spin buffer exchange columns (BioRad) to remove excess DFP. Three microliters of inhibited protein was then diluted into reactivation buffer consisting of 10 mM Tris, pH 8.0, and 10 mM 2-PAM. Samples were incubated overnight at 4 °C, buffer exchanged into 10 mM Tris, pH 8.0, using micro spin columns, and enzymatic activity assays were performed. Fifty microliters of each aliquot (0.56 μg of gVIII-PLA2) was taken for buffer exchange into 10 mM Tris, pH 8.0, for assay with PNPA. It was necessary to remove 2-PAM in this manner as it causes an appreciable background hydrolysis of the assay substrate PNPA. The assays were performed with 920 μL of 50 mM Tris, pH 8.0, 30 μL of 100 mM PNPA in ethanol, and 50 μL of inhibited enzyme.

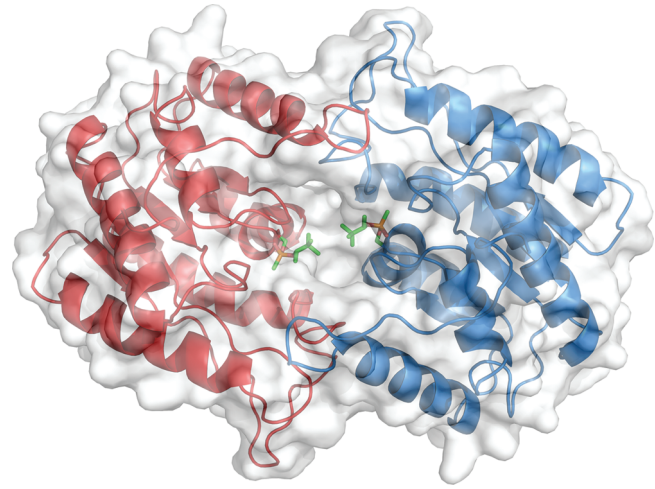

FIGURE 2: Transparent surface and ribbon diagram of the soman complex with the homodimer of gVIII-PLA2. The soman complex and S47 are shown in stick with carbons in green, oxygens in red, and phosphorus in orange. The two subunits (shown in red and blue) are related by crystallographic 2-fold symmetry. Protein interactions from a single subunit contribute to interactions with each S47 and soman adduct. This figure was generated using the program PyMol (*47*).

## RESULTS

*Crystal Structures of Organophosphorus Complexes of gVIII-PLA2.* The refined models of gVIII-PLA2:OP-complexes with paraoxon, soman, and sarin were each solved in the same space group, and the overall protein fold and structures were virtually identical to previously reported structures of the gVIII-PLA2 enzyme (*18, 29, 30*). An alignment of the ligand-free structure with the soman inhibited structure reported here showed a root mean squared deviation of 0.52 Å for all backbone atoms. Furthermore, a comparison of active site residues between ligand-free and the soman-adduct showed little change, with the largest change being a rotation of the H195 side chain moving its NE2 atom by 1.5 Å. The enzyme has crystallized with a single subunit in the asymmetric unit. The physiologically relevant dimeric oligomeric state is formed by taking into account the crystallographic symmetry axis that relates two subunits of the homodimer, as shown in Figure 2. Details of data collection and structural refinement for all three

Table 1: Structure Determination of gVIII-PLA2:OP Complexes

| data collection | paraoxon | soman | sarin |
|---|---|---|---|
| space group | $P3_121$ | $P3_121$ | $P3_121$ |
| cell parameters | | | |
| *a* (Å) | 81.3 | 81.4 | 81.3 |
| *b* (Å) | 81.3 | 81.4 | 81.3 |
| *c* (Å) | 72.5 | 73.0 | 72.8 |
| subunits/asymmetric unit | 1 | 1 | 1 |
| resolution (Å) | 30−2.1 (2.18−2.10) | 30−1.85 (1.92−1.85) | 30−1.85 (1.92−1.85) |
| completeness (%) | 92.1 (90.6) | 96.6 (88.9) | 96.1 (98.2) |
| redundancy | 5.7 (5.5) | 6.5 (3.8) | 5.8 (5.4) |
| $R_{merge}$ [a] | 0.058 (0.354) | 0.079 (0.451) | 0.051 (0.577) |
| refinement | | | |
| resolution range (Å) | 30.0 − 2.10 | 30.0−1.85 | 30.0−1.85 |
| $R_{working}$ [b] | 0.199 | 0.210 | 0.204 |
| $R_{free}$ [b] | 0.206 | 0.228 | 0.231 |
| root mean square deviation | | | |
| bond lengths (Å) | 0.01 | 0.01 | 0.01 |
| bond angles (degrees) | 1.3 | 1.4 | 1.4 |
| total non-hydrogen atoms | 1700 | 1756 | 1788 |
| total water molecules | 82 | 80 | 91 |
| PDB entry code | 3DT6 | 3DT9 | 3DT8 |

[a] $R_{merge} = \Sigma|I_o - I_a|/\Sigma(I_a)$, where $I_o$ is the observed intensity and $I_a$ is the average intensity, the sums being taken over all symmetry related reflections. [b] *R*-factor $= \Sigma|F_o - F_c|/\Sigma(F_o)$, where $F_o$ is the observed amplitude and $F_c$ is the calculated amplitude. $R_{free}$ is the equivalent of $R_{working}$, except it is calculated for a randomly chosen set of reflections that were omitted (5%) from the refinement process (*45*). Values shown in parentheses are for the highest resolution shell.

complexes are summarized in Table 1. All three models include residues 5−216 where the N-terminal (1−4) and C-terminal (217−232) residues were not modeled due to disorder. A ribbon model (Figure 2) of the dimer for gVIII-PLA2 displays a classic α/β-hydrolase fold with a central, parallel, 5-stranded β-sheet surrounded by six α-helices.

Some noteworthy aspects of the gVIII-PLA2 structure include a fold that is significantly different from those of other α/β hydrolases (*31*), a dimer interface composed almost entirely of salt bridges formed by hydrophilic residues (*17*), and two independent active sites that are in close proximity to each other (*17*). This is in contrast to the vast majority of reported intersubunit interfaces, which are usually hydrophobic. The overall tertiary fold and location of key catalytic residues are suggestive of a new hydrolase family defined by the structure of rhamnogalacturonan acetylesterase (*31*). As mentioned earlier the physiological function of gVIII-PLA2 is not well understood (*19, 20*). The dimer interface is composed of salt bridges and hydrogen bonds mostly from the N-terminal helix including Q18/H106, D20/R41, S25/Q143, and R29/Y193 as discussed in detail by Ho et al. (*17*). It has been reported that the dimer can be interrupted by high levels of $CaCl_2$ and that the monomer is not catalytically competent, which provides confirmation of the importance of salt bridges and hydrogen bonds in forming the dimer interface (*32*). A notable aspect of gVIII-PLA2 is the 15 Å deep active site leading to the catalytic triad. The two active sites are in close proximity to each other as shown in the soman complex (Figure 2). Depending on the size of the physiological substrate, it is possible that the two active sites do not operate independently on the yet unidentified physiological substrate. Furthermore, a half-sites reactivity model of these substrates is a topic for future investigations.

*gVIII-PLA2:Paraoxon Complex.* The inhibited complexes were virtually identical to the search model (PDB code 1WAB) except for the additional difference electron density observed contiguous with S47. Sufficient quality difference electron density was present to model in the entire serine-phosphonyl diethyl covalent species (Supplemental Figure 1, Supporting Information). The resulting inhibited complex serves as a mimic for the tetrahedral transition state of an ester substrate following nucleophilic attack by S47. Observed interactions <4 Å between the inhibitor and the enzyme are listed in Table 2 for each OP complex presented. The double bonded phospho oxygen is interacting with the oxyanion hole of the enzyme through H-bonds to the backbone amides of S47, G74 and the side-chain amide of N104. This observation supports the assertion that gVIII-PLA2 may be a member of the SGNH-hydrolase family with an absolutely conserved asparagine serving a key catalytic role (*31*). Typically, hydrolases employing the catalytic triad have contributions from two glycine backbone amides comprising the anion hole. Here we speculate the electronic effects are complemented by the additional coordination with an asparagine side-chain amide.

Table 2: Residue Contacts within 4Å of gVIII-PLA2:OP Complexes

| | paraoxon | | sarin | | soman | |
|---|---|---|---|---|---|---|
| residue/atom type | contact atom[a] | distance (Å) | contact atom[a] | distance (Å) | contact atom[a] | distance (Å) |
| D46, CB | O3 | 3.48 | O1 | 3.28 | O11 | 3.34 |
| ***S47, N***[b] | O3 | 2.96 | O1 | 2.87 | O11 | 2.90 |
| L48, CG | C4 | 3.52 | | | | |
| G73, CA | C1 | 3.42 | C4 | 3.07 | C3 | 3.62 |
| ***G74, N***[b] | O3 | 2.72 | O1 | 2.84 | O11 | 3.02 |
| T103, CG2 | C3 | 3.56 | C1 | 3.57 | C7 | 3.64 |
| **N104, ND2**[b] | O3 | 2.97 | O1 | 2.71 | O11 | 2.75 |
| L194, CD1/CD2 | C4 | 3.63 | C1 | 3.87 | C7 | 3.73 |
| ***H195, NE2*** | O1 | 2.69 | O2 | 2.58 | OH | 3.27 |

[a] Atom types of OP adducts are labeled in Figure 3C for the paraoxon, sarin and soman inhibited enzyme. [b] Residues that show a hydrogen bond with the P═O oxygen of the phosphorus complex. These interactions likely stabilize the oxyanion hole of a tetrahedral intermediate for the reaction. Hydrogen bonds are shown in bold-italics.

One ethyl alkyl substituent was modeled into the acetyl binding pocket formed by L48, T103, and L194. The second ethyl alkyl substituent faces in a direction leading out from the active site gorge to the solvent. Histidine-195 is seen making a H-bond with the phosphoester oxygen of this substituent where H195 is unable to activate a water molecule

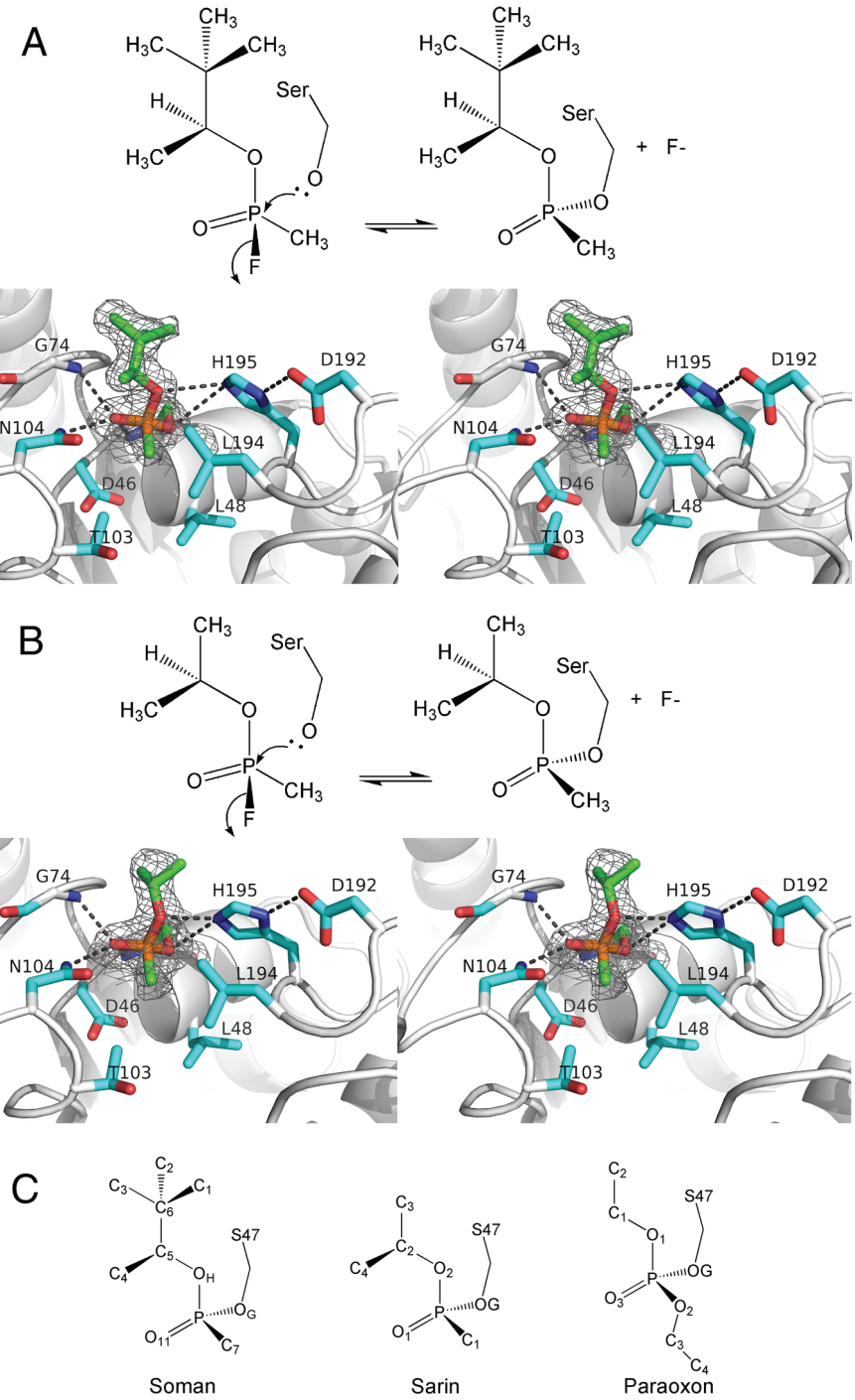


FIGURE 3: The stereoselective reaction of gVIII-PLA2 with soman and sarin. (A) The $P_SC_S$ stereoisomer of soman reacted to give the $P_SC_S$ adduct covalently attached to S47 of the enzyme. Despite the inversion at the phosphorus chiral center, the adduct remains $P_S$ due to the loss of the fluorine atom and nomenclature rules. A stereoview (walleye) of the active site is displayed with a difference electron density map ($2F_o - F_c$ coefficients, 1.2 $\sigma$) around the soman adduct. Active site contact distances are shown in Table 2. (B) The $P_S$ stereoisomer of sarin reacted to give the $P_S$ adduct covalently attached to S47 of the enzyme. A stereoview (walleye) of the active site is displayed with a difference electron density map ($2F_o - F_c$ coefficients, 1.0 $\sigma$) around the sarin adduct. A comparable figure of the paraoxon inhibited complex is presented in Supplemental Figure 1, Supporting Information. (C) The atom names of adducts formed following the inhibition of soman, sarin, and paraoxon are labeled, and their contact distances are reported in Table 2. This figure was generated using the programs Chemdraw and PyMol (*47*).

for catalytic turnover. Presumably, H195 is protonated as a result of proton abstraction from S47 concurrent with nucleophilic attack on paraoxon. This interaction of H195 is analogous to that observed in numerous OP complexes with serine hydrolases (*3, 7, 14*). The direct interaction between H195 and the complexed OP inhibitors precludes H195 from reverting to an unprotonated form and activating a water molecule for a nucleophilic attack and thus regenerating active enzyme.

*gVIII-PLA2:Soman Complex.* The model for the gVIII-PLA2:soman complex shares many of the interactions discussed above for the gVIII-PLA2:paraoxon structure. However, there are a few additional details worth noting. Soman has a total of four stereoisomers due to chiral centers

at the P atom and the $C_\alpha$ of the pinacolyl group (Figure 1). There appears to be only one stereoisomer of the P center bound to the enzyme, as shown in Figure 3. The stereoselectivity appears to be driven by the requirement for the small methyl group to be in the acetyl binding pocket defined by L48, L194, and T103 and for the bulky pinacolyl group to be positioned leading out of the active site gorge. The absolute stereochemistry of the P center in the enzyme-OP complex was determined to be $P_S$. In making this assignment, one must account for the inversion of the stereocenter during the $S_N2$ nucleophilic attack. Also, the priority assignment changes between the unreacted soman and the soman-enzyme adduct due to the substitution of the leaving fluoride group for S47 (Figure 3A). Unequivocal electron density is seen for the three terminal methyl groups of the pinacolyl group, demonstrating that the reaction is stereoselective for the $C_S$ stereocenter as well. Distinct lobes in the electron density can be seen for all the methyl substituents even when the difference electron density map was contoured at 1.2 $\sigma$ as shown in Figure 3A. Furthermore, occupancy refinement did not diverge from 100% occupancy of the soman complex.

The interaction of H195 differs between the paraoxon and the soman complex. In the gVIII-PLA2:paraoxon structure, H195 was seen making an H-bond with a phosphoester oxygen of the OP-adduct. In Figure 3A, it can be seen that H195, despite a close enough contact, is not in the proper geometry to form a H-bond. It appears that the bulky pinacolyl group displaces H195 from its equilibrium position.

*gVIII-PLA2:Sarin Complex.* The model for the gVIII-PLA2:sarin complex shares many of the interactions discussed above for the gVIII-PLA2:paraoxon and soman structures. One difference is that sarin has two stereoisomers due to a chiral center at the phosphorus atom (Figure 1). The stereoselectivity appears to be driven by the requirement for the small methyl group to be in the acetyl binding pocket defined by L48, L194, and T103 and for the larger isopropyl group to be positioned leading out of the active site gorge, just as was found for the pinacolyl group of soman. Also, as in the soman complex, the absolute stereochemistry of the P center in the enzyme−OP complex was assigned as $P_S$. Again, accounting for inversion of the stereocenter during the $S_N2$ nucleophilic attack and substitution of the leaving fluoride group for S47 predicts a stereospecific reactivity of the original sarin molecule of $P_S$ stereochemistry (Figure 3B). Occupancy refinement did not diverge from 100% occupancy for the sarin complex.

*Mass Spectrometry Analysis of OP Inhibited gVIII-PLA2.* While the electron density maps of the gVIII-PLA2:soman and sarin complexes were highly suggestive of full occupancy of nonaged inhibitor, analysis by mass spectrometry was pursued as further proof and to ensure that the electron density was not being misinterpreted. Uninhibited gVIII-PLA2 along with enzyme inhibited by soman, sarin, and DFP were subjected to trypsin digestion and analysis via direct injection into an ESI mass spectrometer. Table 3 shows the predicted masses for the peptide comprising residues 30−59 modified with sarin, soman, and DFP compared to the unmodified protein. The predicted masses of nonaged and aged complexes of this peptide were compared to mass spectra measured. Figure 4 shows the ESI mass spectra obtained for soman and sarin complexes. The presence of a peak consistent with a nonaged adduct and the absence of either the unmodified peak and a peak of the size predicted for an aged product further support the identity of nonaged soman and sarin adducts in the complexes. The ESI mass spectra for unmodified gVIII-PLA2 and DFP reacted enzyme are presented in Supplemental Figure 2, Supporting Information. The unmodified gVIII-PLA2 sample showed a peak consistent with the predicted mass of an unmodified S47, and the DFP spectra are likewise consistent with the identity of a nonaged enzyme complex with a DFP adduct.

Table 3: Predicted Masses of gVIII-PLA2 Peptide (30−59) Modified with OP Inhibitors

| | $M + H^+$ | $M + 2H^{2+}$ | $M + 3H^{3+}$ | $M + 4H^{4+}$ |
|---|---|---|---|---|
| unmodified | 3578.1 | 1789.5 | 1193.4 | ***895.3***[a] |
| soman complex[b] | | | | |
| nonaged | 3740.0 | 1870.5 | 1247.3 | ***935.7*** |
| aged | 3656.0 | 1828.5 | 1219.3 | 914.7 |
| sarin complex[b] | | | | |
| nonaged | 3698.0 | 1849.5 | 1233.3 | ***925.2*** |
| aged | 3656.0 | 1828.5 | 1219.3 | 914.7 |
| DFP complex[c] | | | | |
| nonaged | ***3739.8*** | | | |
| aged | 3697.8 | | | |

[a] Masses highlighted in bold-italics were observed in the mass spectra of the gVIII-PLA2 trypsin digests. [b] Masses reported are average isotopic masses. [c] Masses reported are monoisotopic masses.

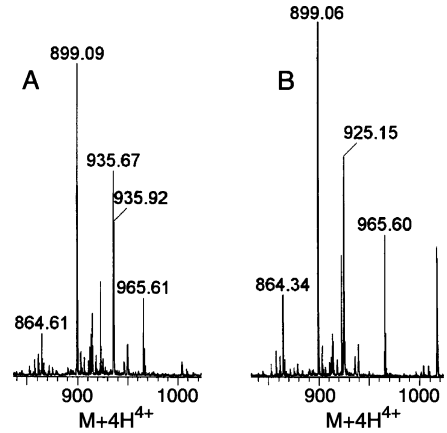


FIGURE 4: Electrospray ionization mass spectra of trypsin digest of gVIII-PLA2 reacted with the nerve agents soman and sarin. (A) The peak at 935.67 *m*/*z* is a close match for the 30−59 peptide containing the active site S47 covalently modified with nonaged soman. Furthermore, there is no major peak at 895.3 *m*/*z* as shown in Supplemental Figure 2, Supporting Information for the unmodified 30−59 peptide. Also, there is no major peak at 914.7 *m*/*z* that would indicate the presence of the aged product. (B) Mass spectra of trypsin digest of sarin inhibited gVIII-PLA2. The peak at 925.15 *m*/*z* is a close match for the 30−59 peptide containing the active site S47 covalently modified with nonaged sarin. There is no major peak at 914.7 *m*/*z* that would indicate the presence of the aged product.

*Analysis of Stereoselectivity by Reaction with Racemic Sarin.* We have studied stereoselective binding of sarin to gVIII-PLA2 by GC/MS using a chiral chiraldex gamma-cyclodextrin trifluoroacetyl column that can separate the $P_S$ and $P_R$ stereoisomers of sarin (*28*). Figure 5 shows the traces of unreacted and sarin-enzyme reacted samples following the reaction with roughly a 600-fold excess of enzyme to sarin. Prior experiments with human BChE have assigned the right-most peak as the $P_S$ stereoisomer of sarin (not shown). Following reaction, there is less deflection of the $P_S$ peak (∼13%) indicating preferential binding of this stereoisomer. This qualitatively is consistent with the crystal-

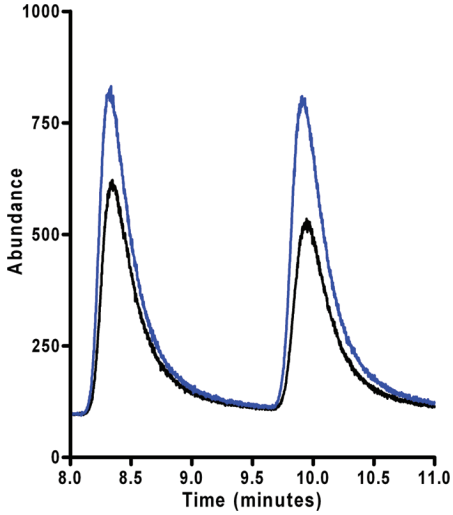


FIGURE 5: Chiral analysis of the reaction of gVIII-PLA2 with racemic sarin. The top trace (blue) is an injection of sarin in buffer only. The bottom trace (black) is an injection following incubation of sarin with gVIII-PLA2. Both control and gVIII-PLA2 samples were incubated for 30 min at room temperature before extraction and isolation of the unbound sarin. Previous experiments involving coincubation of human BChE with racemic sarin indicated that the $P_S$ isomer has a retention time close to 10 min (right peak in figure). The differences between the blue and black traces is the result of bulk binding of both stereoisomers of sarin by the gVIII-PLA2; a minor preference for the $P_S$ isomer (~13% difference) was detected.

lographic data, which likewise supports a stereochemical preference of gVIII-PLA2 for the $P_S$ stereoisomer of sarin.

*Reactivation Attempts with Oxime.* A premise of a nonaged OP complex is that nucleophiles, such as oximes, often reactivate the enzyme. Further evidence for a nonaged complex was investigated by attempting oxime reactivation by 2-PAM of gVIII-PLA2 enzyme that had been OP-inactivated. All attempts to reactivate DFP inhibited gVIII-PLA2 by incubation with 2-PAM failed to recover any significant activity as measured against 3 mM PNPA in 10 mM Tris, pH 8.0. This procedure was performed several times and in all cases a slope of less than 100 mOD/min at 400 nm was found, which was attributed to our lower level of detection due to background hydrolysis from residual 2-PAM.

## DISCUSSION

There is considerable controversy regarding the physiological function of gVIII-PLA2 (*19, 20*). The gVIII-PLA2 enzyme from bovine brain had been previously named as the catalytic domain of type-Ib PAF-AH (*16*). The most recent published structural data for gVIII-PLA2 is a structure of a heterotetramer, which has the homodimer of the catalytic doman in the center, and is flanked by a beta-propeller regulatory domain on each side (*18*). It is significant that gVIII-PLA2 has no sequence homology to the other PAF-AH enzymes. Although structures of gVIII-PLA2 inhibited by OPs do not definitively serve in identifying the physiological substrates of gVIII-PLA2, they do provide clues to important interactions of the putative hydrolase mechanism. Here the OP inhibited structures help describe the limits of the possible modes of substrate binding. Figure 2 shows the molecular surface for the dimer gVIII-PLA2:soman complex. The two covalently linked OP inhibitors fill the entire volume at the back of the active site pocket. Because of the location of the double bonded oxygen of the OP moiety in the oxyanion hole and the small methyl substituent in the acetyl binding pocket, the only possible position for the bulky alkyl groups of the soman and sarin complexes is leading out of the active site toward the solvent. The same steric restrictions would apply to the covalent acyl intermediate formed when the enzyme binds to its putative substrate PAF. Therefore, the only probable locations for the choline binding element are on the surface of the active site leading to the solvent or across the dimer interface into the second active site. It is clear from these structures and preliminary docking studies that only a single substrate molecule of PAF could possibly bind to the dimer containing two neighboring active sites.

Although gVIII-PLA2 has been referred to as PAF-AH in numerous publications, no convincing evidence (*19, 20*) exists to support a function of the enzyme that PAF or even any other phospholipid is an endogenous substrate. Additionally, previous studies did not reveal a strict preference for a specific phospholipid headgroup on the substrate (*33*). Therefore, it is not surprising that gVIII-PLA2 lacks a structural element that is specifically responsible for strong binding of the phospholipid headgroup. Our structure supports this train of thought, where the phospho-headgroup of a phospholipid substrate is predicted to point toward the solvent. The gVIII-PLA2 enzyme is water-soluble and has not been reported to interact with membrane or membrane-like interfaces. This is in contrast to a model of PAF-AH specificity and interface binding presented for the enzyme plasma PAF-AH (*34*). Here, the phospholipid interface presents the substrate PAF into the active site of PAF-AH which is tightly associated with membranes and membrane-like surfaces.

The most intriguing observation of the present work is the lack of observable aging of the soman and sarin complexes with gVIII-PLA2, as shown by the crystallographic and mass spectrometry results. The lack of aging in the gVIII-PLA2:sarin complex is particularly perplexing due to an apparently ideal orientation of the active site H195 to carry out proton transfer and catalyze the aging process. The majority of serine hydrolases have been demonstrated to promote the aging reaction when reacted with branched OPs, such as trypsin-DFP (*35*), chymotrypsin-DFP (*36*), *S. scabies* esterase-DFP, and AChE complexes with sarin, soman or DFP (*37*). These enzymes have in common a catalytic histidine to carry out proton transfer and a solvent-accessible active site. Several OP complex crystal structures in aged and nonaged forms allow us to compare active site features in order to look for a trend that could explain the determinants of OP aging. Table 4 summarizes for these complexes a comparison of the position of the catalytic histidine to the oxygen adjacent to the alkyl group that either ages or not. The most notable comparison is between the nonaged sarin complexes with AChE (*38*) and gVIII-PLA2. Although each displays an H-bond, the gVIII-PLA2 His-O distance is much shorter and stronger at 2.58 Å. This shorter H-bond may restrict histidine from participating in a solvent mediate aging mechanism. The mobility of the histidine in the AChE enzyme has been previously argued to be critical to explain its broad specificity and rapid rates of reaction (*6*). Other features of the active-site of gVIII-PLA2 may play a key role in the apparent slow aging rate for the gVIII-

Table 4: Comparison of OP-His Distance and Changes in Surface Area for OP Complexes

| | distance between[a] His and OP oxygen (Å) | ΔASA[b] (Å$^2$) | PDB codes of[c] OP complexes |
|---|---|---|---|
| AChE-sarin, nonaged | 3.19 | 95.5 | 2jgg, 1j06 |
| AChE-sarin, aged | 2.93 | | 1cfj |
| AChE-DFP, nonaged | 2.86 | | 2jgi |
| CE1-soman, nonaged | 5.18 | 77.5 | 2hrq, 2h7c |
| BuChE-soman, aged | 2.89 | | 1p0p |
| BuChE-soman, aged | 2.86 | | 1p0q |
| gVIII-PLA2:paraoxon, nonaged | 2.69 | 59.3 | 3dt6, 1wab |
| gVIII-PLA2:sarin, nonaged | 2.58 | 82.0 | 3dt8, 1wab |
| gVIII-PLA2:soman, nonaged | 3.27 | 99.0 | 3dt9, 1wab |

[a] The distance between the catalytic histidine to the oxygen adjacent to the alkyl group that did age (aged complexes) or did not age (nonaged complexes) is listed. [b] The change in accessible surface area (ΔASA) (*46*) of residues in contact with OPs was calculated with respect to residues in the ligand-free enzyme structure with units of Å$^2$. [c] The first code of the pair is the nonaged complex and the second is the ligand-free form that it is compared to for the ΔASA calculation. Nonaged complexes have a single PDB code listed.

PLA2:sarin complex. Unlike the active site of AChE, the gVIII-PLA2 active site does not have any tryptophan residues neighboring the OP complex. The cation-$\pi$ interaction of W86 in AChE is believed to stabilize a carbocation intermediate (*39*) as described in Figure 1. Likewise, E202 in human AChE is thought to play a role in "aging" in the cholinesterases. Substitution of Glu to Gln at this position results in a variant protein that does not age with soman (*15*). Neither carboxylesterase (*9*) nor gVIII-PLA2 have a comparable Glu or Asp residue that could participate in stabilization of a carbocation intermediate. The absence of both a carboxylate and a tryptophan residue from the active site of gVIII-PLA2 may be the key factors that explain a lack of aging observed. Aging is slow when compared to almost all other enzyme-mediated processes. In light of the consensus mechanism for aging shown in Figure 1, this is not surprising since a carbocation must be formed by charge separation. Aging rates have been previously rationalized based on the ability of the developing carbocation to be directly stabilized by the enzyme active site (*11*). Therefore, it is reasonable to assume that the dielectric of the surroundings and the presence or absence of cation-$\pi$ or other charge−charge interactions would be a factor in the ability of the carbocation to form and be stabilized.

While being fundamentally similar to the gVIII-PLA2:paraoxon and gVIII-PLA2:soman complexes, the gVIII-PLA2:sarin complex is the most novel of the three OP complexes reported here. Although enzyme−OP conjugates with unbranched alkyl groups have some propensity to age, their aging rates are typically much slower than those observed with OP compounds with branched alkyl groups. Therefore, the presence of a nonaged complex in the gVIII-PLA2:paraoxon complex was not particularly surprising. The nonaged gVIII-PLA2:soman complex may have a simple explanation due to the displacement of H195 from a functionally relevant position in this structure; this suggests that proper positioning of H195 may be necessary to carryout proton transfer to the OP moiety required for aging. Likewise, the recently published structure of human CE1 in nonaged complexes with soman and tabun was explained due to a rather long His-OP oxygen distance (*9*). In the CE1−soman complex this distance was 5.2 Å and the histidine was positioned on the opposite side of the alkyl group that would undergo an aging reaction. Unlike the other complexes mentioned above, the gVIII-PLA2:sarin complex (Figure 3B) appears to have all the elements necessary for aging, including H195 in a position to carryout proton transfer. The lack of any observable aging for the gVIII-PLA2:sarin complex was a puzzling observation. Aging rates vary over a wide range; however, aged complexes had always been observed for X-ray structural determinations prior to the recent work on human CE1 (*9*) and the present work. While no quantitative study was conducted, the results presented here suggest that the half-life for aging in the gVIII-PLA2:sarin complex, which was solved using crystals that were incubated at room temperature for 2 weeks, is significantly longer than the 10 day half-life seen for the chymotrypsin-DFP complex (*13*).

Aging rates have been quantitated previously by measuring the ability of a second nucleophile, typically oximes such as 2-PAM, to reactivate nonaged enzyme (*27*). In cases where OP inhibited enzymes are reactivated by oximes, aging is indicated by an inability to recover 100% of the enzyme activity. For the complexes of gVIII-PLA2, the stability of nonaged complexes in 2 week old protein crystals and mass spectrometry results gave unequivocal evidence of an extremely slow aging process. Therefore, we investigated whether 2-PAM would reactivate these gVIII-PLA2 complexes that had been inhibited by the OP compound DFP. Oxime reactivation was qualitatively assessed by incubation with 10 mM 2-PAM over the course of several hours. However, no reactivation was observed despite the knowledge that DFP-inhibited gVIII-PLA2 does not display any evidence of aging over this time span as determined by mass spectrometry. The simplest explanation for this observation is that the phosphorus atom of the inhibitor was made inaccessible to the oxime nucleophile by the shape of the active site and the steric exclusion by the isopropyl group. Steric barriers to rearrangement of a nonaged complex were proposed to be a critical component to explain the aging rates of sarin in AChE (*38*). We have made a comparison of our nonaged sarin complex of gVIII-PLA2 with the nonaged complex of sarin to mouse AChE (*38*) (Supplemental Figure 3, Supporting Information). The isopropyl group in the gVIII-PLA2 is packed closer to the van der Waals surface of the active site compared to the AChE structure. This implies greater mobility of the isopropyl group in AChE, and therefore greater conformational access to the isopropyl oxygen and phosphorus atom of the sarin nonaged adduct. Also, as discussed above, a short H-bond of 2.6 Å between H195 and the oxygen adjacent to the aging alkyl group may limit motion by this residue, and thereby restrict its ability to participate in aging reactions or in oxime reactivation. Recently, Carletti et al. (*40*) reported the structures of human BChE complexed with the nerve agent tabun in both a nonaged and aged form; these structures lay a framework to better understand structural requirements of oxime activation and the ultimate optimization of a reactivation strategy.

The theoretical groundwork has been laid to establish the mechanism behind the aging phenomenon (*6, 10, 11*). In the present work, gVIII-PLA2 has been identified as an enzyme that apparently has a mechanism to thwart the aging that has been thought to universally occur with serine hydrolases inhibited with OP compounds. The hypothesis that a low

dielectric in the active site of the inhibited gVIII-PLA2 complex together with the lack of cation-$\pi$ interactions and a properly placed carboxylate side chain to stabilize a carbocation are responsible for inhibiting aging is in theoretical agreement with the established carbocation mechanism for aging (*11*). Conversely, one could argue it may be that the inability to age is the natural rule for these hydrolases and that aging in AChE and BuChE is the exception. Regardless, these observations are useful to guide the engineering of enzymes to display OP hydrolase activity, as these approaches have enjoyed limited success (*12, 41*). The development of such an OP hydrolase would have great potential utility as a treatment for OP intoxication.

The $P_S$ stereoselectivity of the soman and sarin complexes with gVIII-PLA2 make this enzyme an attractive target to develop as a catalytic bioscavenger, since it matches the toxicity profile of these agents with AChE (*42*). The stereoselectivity of gVIII-PLA2 is controlled by the acyl chain binding pocket and oxyanion hole comprised of the backbone amides of G74 and S47 and the side chain amide N104 of gVIII-PLA2 (Figure 3). The crystal structures of soman and sarin complexes, together with the GC/MS chiral column analysis, demonstrate a stererochemical preference for $P_S$ stereoisomers. This coupled with a lack of detectable aging makes protein engineering feasible to design a catalytic bioscavenger of the more toxic $P_S$ isomer. This approach contrasts other catalytic bioscavengers in development that utilize a mechanism in which the initial attack is by a catalytic water molecule. The enzymes paraoxonase 1 (*43*) and bacterial phosphotriesterase (*44*) have shown the most promise here. However, despite notable catalytic efficiencies, these enzymes have high values of $K_M$; therefore, they suffer from an inability to bind OP compounds at concentrations shown to be lethal. The extensive interactions between the oxyanion hole of gVIII-PLA2 and the OP adducts of soman and sarin potentially allow the development of a catalytic hydrolase, which would have a considerably lower $K_M$ value and stereoselective preference for the more toxic OP isomers. Group-VIII PLA2 and enzymes with similar properties are currently being exploited to develop a stereoselective and catalytic bioscavenger of highly toxic OPs that will work at the physiologically relevant and low concentrations of OPs that are known to be toxic.

## ACKNOWLEDGMENT

We thank John Dykins, director of the mass spectrometry facility in the Department of Chemistry and Biochemistry at the University of Delaware, for assistance with data collection.

## SUPPORTING INFORMATION AVAILABLE

Supplemental Figure 1: the inhibition of gVIII-PLA2 with paraoxon as a diethyl phosphonyl adduct covalently attached to S47 of the enzyme; supplemental Figure 2: mass spectra of trypsin digest of gVIII-PLA2 in a ligand free form and reacted with DFP; and supplemental Figure 3: a comparison of the van der Waals surfaces of nonaged sarin complexes in gVIII-PLA2 and AChE enzymes. This material is available free of charge via the Internet at http://pubs.acs.org.

## REFERENCES

1. Casida, J. E., and Quistad, G. B. (2004) Organophosphate toxicology: safety aspects of nonacetylcholinesterase secondary targets. *Chem. Res. Toxicol. 17*, 983–998.
2. Millard, C. B., Kryger, G., Ordentlich, A., Greenblatt, H. M., Harel, M., Raves, M. L., Segall, Y., Barak, D., Shafferman, A., Silman, I., and Sussman, J. L. (1999) Crystal structures of aged phosphonylated acetylcholinesterase: nerve agent reaction products at the atomic level. *Biochemistry 38*, 7032–7039.
3. Broomfield, C. A., Lockridge, O., and Millard, C. B. (1999) Protein engineering of a human enzyme that hydrolyzes V and G nerve agents: design, construction and characterization. *Chem. Biol. Interact. 119−120*, 413–418.
4. Michel, H. O., Hackley, B. E., Berkowitz, L., List, G., Hackley, E. B., Gilliam, W., and Paukan, M. (1967) Ageing and dealkylation of Soman (pinacolylmethylphosphonofluoridate)-inactivated eel cholinesterase. *Arch. Biochem. Biophys. 121*, 29–34.
5. Harris, L. W., Fleisher, J. H., Clark, J., and Cliff, W. F. (1966) Dealkylation and loss of capacity for reactivation of cholinesterase inhibited by sarin. *Science 154*, 404–407.
6. Millard, C. B., Koellner, G., Ordentlich, A., Shafferman, A., Silman, I., and Sussman, J. L. (1999) Reaction products of acetylcholinesterase and VX reveal a mobile histidine in the catalytic triad. *J. Am. Chem. Soc. 121*, 9883–9884.
7. Nachon, F., Asojo, O. A., Borgstahl, G. E. O., Masson, P., and Lockridge, O. (2005) Role of water in aging of human butyrylcholinesterase inhibited by echothiophate: the crystal structure suggests two alternative mechanisms of aging. *Biochemistry 44*, 1154–1162.
8. Cole, L. B., Chu, N., Kilpatrick, M., Volanakis, J. E., Narayana, S. V. L., and Babu, Y. S. (1997) Structure of diisopropyl fluorophosphate-inhibited factor D. *Acta Crystallogr. D53* 143–150.
9. Fleming, C. D., Edwards, C. C., Kirby, S. D., Maxwell, D. M., Potter, P. M., Cerasoli, D. M., and Redinbo, M. R. (2007) Crystal structures of human carboxylesterase 1 in covalent complexes with the chemical warfare agents soman and tabun. *Biochemistry 46*, 5063–5071.
10. Shafferman, A., Ordentlich, A., Barak, D., Stein, D., Areil, N., and Velan, B. (1996) Aging of phosphylated human acetylcholinesterase: catalytic processes mediated by aromatic and polar residues of the active centre. *Biochem. J. 318−840*, 833.
11. Barak, D., Ordentlich, A., Segall, Y., Velan, B., Benschop, H. P., De Jong, L. P. A., and Shafferman, A. (1997) Carbocation-mediated processes in biocatalysts. Contribution of aromatic moieties. *J. Am. Chem. Soc. 119*, 3157–3158.
12. Lockridge, O., Blong, R. M., Masson, P., Froment, M. T., Millard, C. B., and Broomfield, C. A. (1997) A single amino acid substitution, Gly117His, confers phosphotriesterase (organophosphorus acid anhydride hydrolase) activity on human butyrylcholinesterase. *Biochemistry 36*, 786–795.
13. van der Drift, A. C. M., Beck, H. C., Dekker, W. H., Hulst, A. G., and Wils, E. R. J. (1985) P-NMR and mass spectrometry of atropinesterase and some serine proteases phosphorylated with a transition-state analogue. *Biochemistry 24*, 6894–6903.
14. Harel, M., Su, C.-T., Frolow, F., Ashani, Y., Silman, I., and Sussman, J. L. (1991) Refined crystal structures of "aged" and "non-aged" organophosphoryl conjugates of gamma-chymotrypsin. *J. Mol. Biol. 221*, 909–918.
15. Shafferman, A., Ordentlich, A., Barak, D., Stein, D., Ariel, N., and Velan, B. (1996) Aging of phosphylated human acetylcholinesterase: catalytic processes mediated by aromatic and polar residues of the active centre. *Biochem. J. 318 (Pt 3)*, 833–840.
16. Arai, H. (2002) Platelet-activating factor acetylhydrolase. *Prostaglandins Other Lipid Mediat. 68−69*, 83–94.
17. Ho, Y. S., Swenson, L., Derewenda, U., Serre, L., Wei, Y., Dauter, Z., Hattori, M., Adachi, T., Aoki, J., Arai, H., Inoue, K., and Derewenda, Z. S. (1997) Brain acetylhydrolase that inactivates platelet-activating factor is a G-protein-like trimer. *Nature (London) 385*, 89–93.
18. Tarricone, C., Perrina, F., Monzani, S., Massimiliano, L., Kim, M. H., Derewenda, Z. S., Knapp, S., Tsai, L. H., and Musacchio, A. (2004) Coupling PAF signaling to dynein regulation: structure of LIS1 in complex with PAF-acetylhydrolase. *Neuron 44*, 809–821.
19. Derewenda, Z. S. (2002) Substrate-selectivity in acylhydrolases: a cautionary tale. *Colloids Surfaces B: Biointerfaces 26*, 31–35.

20. Epstein, T. M. (2005) Structural and kinetic studies of two enzymes catalyzing phospholipase A2 activity, Ph.D. Thesis, in Biochemistry, University of Delaware, Newark.
21. Otwinowski, Z., and Minor, W. (1997) Processing of X-ray diffraction data collected in oscillation mode. *Methods Enzymol. 276*, 307–326.
22. Brunger, A. T., Adams, P. D., Clore, G. M., Delano, W. L., Gros, P., Grosse-Kunstleve, R. W., Jiang, J.-S., Kuszewski, J., Nilges, N., Pannu, N. S., Read, R. J., Rice, L. M., Simonson, T., and Warren, G. L. (1998) Crystallography and NMR systems (CNS): A new software system for macromolecular structure determination. *Acta Crystallogr., Sect. D 54*, 905–921.
23. Murshudov, G. N., Vagin, A. A., and Dodson, E. J. (1997) Refinement of macromolecular structures by the maximum-likelihood method. *Acta Crystallogr., Sect. D 53*, 240–255.
24. Jones, T. A., Zou, J. Y., Cowan, S. W., and Kjeldgaard, M. (1991) Improved methods for building protein models in electron density maps and the location of errors in these models. *Acta Crystallogr., Sect. A 47*, 110–119.
25. Emsley, P., and Cowtan, K. (2004) Coot: model-building tools for molecular graphics. *Acta Crystallogr. Sect. D 60*, 2126–2132.
26. CCP4. (1994) The CCP4 Suite: Programs for Protein Crystallography, *Acta Crystallogr. Sect. D 50*, 760−763.
27. Masson, P., Fortier, P. L., Albaret, C., Froment, M. T., Bartels, C. F., and Lockridge, O. (1997) Aging of di-isopropyl-phosphorylated human butyrylcholinesterase. *Biochem. J. 327*, 601–607.
28. Yeung, D. T., Smith, J. R., Sweeney, R. E., Lenz, D. E., and Cerasoli, D. M. (2007) Direct detection of stereospecific soman hydrolysis by wild-type human serum paraoxonase. *FEBS J. 274*, 1183–1191.
29. Barak, R., Ordentlich, A., Barak, D., Fischer, M., Benschop, H. P., De Jong, L. P., Segall, Y., Velan, B., and Shafferman, A. (1997) Direct determination of the chemical composition of acetylcholinesterase phosphonylation products utilizing electrospray-ionization mass spectrometry. *FEBS Lett. 407*, 347–352.
30. Sheffield, P. J., McMullen, T. W., Li, J., Ho, Y. S., Garrard, S. M., Derewenda, U., and Derewenda, Z. S. (2001) Preparation and crystal structure of the recombinant alpha(1)/alpha(2) catalytic heterodimer of bovine brain platelet-activating factor acetylhydrolase Ib. *Protein Eng. 14*, 513–519.
31. Molgaard, A., Kauppinen, S., and Larsen, S. (2000) Rhamnogalacturonan acetylesterase elucidates the structure and function of a new family of hydrolases. *Structure 8*, 373–383.
32. McMullen, T. W., Li, J., Sheffield, P. J., Aoki, J., Martin, T. W., Arai, H., Inoue, K., and Derewenda, Z. S. (2000) The functional implications of the dimerization of the catalytic subunits of the mammalian brain platelet-activating factor acetylhydrolase (Ib). *Protein Eng. 13*, 865–871.
33. Manya, H., Aoki, J., Kato, H., Ishii, J., Hino, S., Arai, H., and Inoue, K. (1999) Biochemical characterization of various catalytic complexes of the brain platelet-activating factor acetylhydrolase. *J. Biol. Chem. 274*, 31827–31832.
34. Samanta, U., and Bahnson, B. J. (2008) Crystal structure of human plasma platelet-activating factor acetylhydrolase: structural implication to lipoprotein binding and catalysis. *J. Biol. Chem. 283*, 31617–31624.
35. Kossiakoff, A. A. (1984) *Basic Life Sci. 27*, 281–304.
36. Harel, M., Su, C.-T., Frolow, F., Ashani, Y., Silman, I., and Sussman, J. L. (1991) *J. Mol. Biol. 221*, 909–918.
37. Millard, C. B., Kryger, G., Ordentlich, A., Greenblatt, H. M., Harel, M., Raves, M. L., Segall, Y., Barak, D., Shafferman, A., Silman, I., and Sussman, J. L. (1999) *Biochemistry 38*, 7032–7039.
38. Hornberg, A., Tunemalm, A. K., and Ekstrom, F. (2007) Crystal structures of acetylcholinesterase in complex with organophosphorus compounds suggest that the acyl pocket modulates the aging reaction by precluding the formation of the trigonal bipyramidal transition state. *Biochemistry 46*, 4815–4825.
39. Ordentlich, A., Barak, D., Kronman, C., Benschop, H. P., De Jong, L. P., Ariel, N., Barak, R., Segall, Y., Velan, B., and Shafferman, A. (1999) Exploring the active center of human acetylcholinesterase with stereomers of an organophosphorus inhibitor with two chiral centers. *Biochemistry 38*, 3055–3066.
40. Carletti, E., Li, H., Li, B., Ekstrom, F., Nicolet, Y., Loiodice, M., Gillon, E., Froment, M. T., Lockridge, O., Schopfer, L. M., Masson, P., and Nachon, F. (2008) Aging of cholinesterases phosphylated by tabun proceeds through O-dealkylation, *J. Am. Chem. Soc. 130*, 16011−16020.
41. Millard, C. B., Lockridge, O., and Broomfield, C. A. (1998) Organophosphorus acid anhydride hydrolase activity in human butyrylcholinesterase: synergy results in a somanase. *Biochemistry 37*, 237–247.
42. Benschop, H. P., Konings, C. A., Van Genderen, J., and De Jong, L. P. (1984) Isolation, anticholinesterase properties, and acute toxicity in mice of the four stereoisomers of the nerve agent soman. *Toxicol. Appl. Pharmacol. 72*, 61–74.
43. Amitai, G., Gaidukov, L., Adani, R., Yishay, S., Yacov, G., Kushnir, M., Teitlboim, S., Lindenbaum, M., Bel, P., Khersonsky, O., Tawfik, D. S., and Meshulam, H. (2006) Enhanced stereoselective hydrolysis of toxic organophosphates by directly evolved variants of mammalian serum paraoxonase. *FEBS 273*, 1906–1919.
44. Ghanem, E., and Raushel, F. M. (2005) Detoxification of organophosphate nerve agents by bacterial phosphotriesterase. *Toxicol. Appl. Pharmacol. 207*, 459–470.
45. Brunger, A. T. (1992) The free R value: A novel statistical quantity for assessing the accuracy of crystal structures. *Nature (London) 355*, 472–474.
46. Lee, B., and Richards, F. M. (1971) The interpretation of protein structures: estimation of static accessibility. *J. Mol. Biol. 55*, 379–400.
47. DeLano, W. L. (2002) *The PyMOL User's Manual*, DeLano Scientific, Palo Alto, CA, USA.


BI8023527